JACS
JOURNAL OF THE AMERICAN CHEMICAL SOCIETY
Article
pubs.acs.org/JACS

Role of Gold(I) α-Oxo Carbenes in the Oxidation Reactions of Alkynes Catalyzed by Gold(I) Complexes

Jiří Schulz, Lucie Jašíková, Anton Škríba, and Jana Roithová*

Department of Organic Chemistry, Faculty of Science, Charles University in Prague, Hlavova 2030, 128 43 Prague 2, Czech Republic

Supporting Information

ABSTRACT: The gas phase structures of gold(I) complexes formed by intermolecular oxidation of selected terminal (phenylacetylene) and internal alkynes (2-butyne, 1-phenylpropyne, diphenylacetylene) were investigated using tandem mass spectrometry and ion spectroscopy in conjunction with quantum-chemical calculations. The experiments demonstrated that the primarily formed β-gold(I) vinyloxypyridinium complexes readily undergo rearrangement, dependent on their substituents, to either gold(I) α-oxo carbenenoids (a synthetic surrogate of the α-oxo carbenes) or pyridine adducts of gold(I) enone complexes in the condensed phase and that the existence of naked α-oxo carbenes is highly improbable. Isotopic labeling experiments performed with the reaction mixtures clearly linked the species that exist in solution to the ions transferred to the gas phase. The ions were then fully characterized by CID experiments and IRMPD spectroscopy. The conclusions based on the experimental observations perfectly correspond with the results from quantum-chemical calculations.

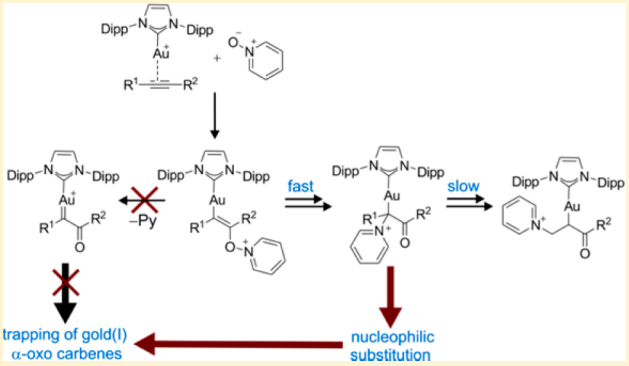

INTRODUCTION

Gold(I) α-oxo carbenes have been suggested as intermediates in the oxidation reactions of alkynes by using mild organic oxidants such as *N*-oxides, sulfoxides or nitrones (Scheme 1).[1] The initial addition of an oxygen nucleophile (e.g., pyridine *N*-oxide) is followed by an expulsion of a leaving group (i.e., pyridine), resulting in a formation of the respective gold(I) α-oxo carbenes.[2,3] These elusive species are strong electrophiles and thus may be conveniently trapped by a reaction with various nucleophiles. The reported procedures involve mostly intramolecular trapping,[4] but several intermolecular reactions have been reported as well.[5]

Most of the reactions between the elusive gold(I) α-oxo carbenes and nucleophiles have been reported for the carbenes generated from terminal alkynes (R′ = H in Scheme 1).[4,5] Gold(I) α-oxo carbenes substituted by an alkyl group R′ having a hydrogen atom bound to the carbon atom directly neighboring with the carbene carbon atom can alternatively undergo a hydrogen rearrangement resulting in the formation of α,β-unsaturated ketones (cf. Scheme 1).[6]

Scheme 1. Proposed Formation of Gold(I) α-Oxo Carbenes and Their Transformation to Final Products

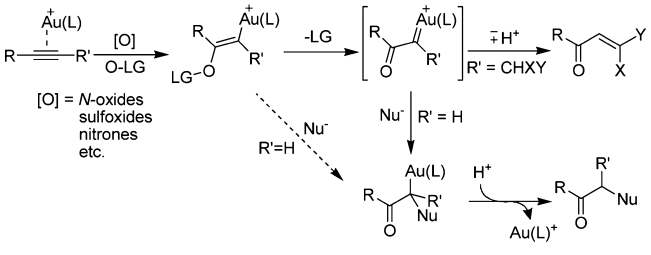

The intermediacy of the gold(I) α-oxo carbenes has been recently questioned in several intramolecular reactions.[7] If the substituent R (cf. Scheme 1) contains a nucleophilic group, which is nearby and can immediately participate in the process of the elimination of the leaving group, the invoking of the α-oxo carbene formation is not necessary (dashed arrow in Scheme 1).

During the past decade, mass spectrometry proved to be a highly versatile tool for trapping of elusive species such as low abundant and unstable reaction intermediates.[8] Electrospray ionization mass spectrometry (ESI-MS) offers not only a highly sensitive technique for monitoring of complex reaction mixtures, but it can also be supported by another advanced experimental technique such as ion spectroscopy,[9,10] that may provide additional information about the structure of sampled species in the gas phase. We have applied tandem mass spectrometry, infrared multiphoton dissociation spectroscopy (IRMPD) and density functional theory (DFT) calculations in order to trap potential reaction intermediates in the gold(I) mediated oxidations of alkynes, to probe the structure of the isolated intermediates in the gas phase and to unravel the role of gold(I) α-oxo carbenes in these reactions.

Received: June 13, 2014
Published: July 28, 2014

dx.doi.org/10.1021/ja505945d | J. Am. Chem. Soc. 2014, 136, 11513−11523

EXPERIMENTAL AND COMPUTATIONAL DETAILS

The mass spectrometry measurements were performed with a Finnigan LCQ Deca ion trap mass spectrometer.[11] The mass spectrometer is equipped with a conventional ESI source consisting of a spray unit that is followed by a heated capillary, a first set of lenses that allows setting of soft or hard ionization conditions by varying the degree of collisional activation in the medium-pressure regime, and two transfer octopoles. Generated ions are stored within a Paul ion trap, which also allows a further manipulation including various MS^n experiments. For detection, the ions are ejected from the ion trap to an electron multiplier. The collisional activation in CID experiments is achieved by collisions with helium buffer gas (pressure of He within the ion trap is $\sim 10^{-3}$ mbar) induced by applying of an excitation AC voltage to the end-caps of the ion trap. Generally, the mass spectra were collected using soft ionization conditions with the heated capillary kept at 150 °C, the spraying voltage set to 6 kV and flow rate of 5.0 μL min^{-1}. For the CID experiments an excitation period of 30 ms and a trapping parameter $q_z = 0.25$ was used. As the excitation of mass selected ions for CID experiments may be influenced also by the chosen isolation width, we used uniformly the isolation width of 2 amu for all MS^2 experiments (being generally sufficient for separation of single isotops) and 4 amu for the second stage of mass selection during MS^3 experiments. The experimental appearance energies (AEs) of the observed fragmentation channels were extracted from the energy resolved CID experiments applying a recently introduced approach for calibration of the collision-energy scale.[12,13] This calibration scheme is based on the correlation of experimental AEs of a set of the reference ions with the values obtained by theoretical calculations. The breakdown curves were modeled by sigmoid functions using a least-squares method. The AEs are then obtained by a linear extrapolation of the rise of the sigmoid functions at $E_{1/2}$ to the baseline. The intensities due to the ions formed by consecutive dissociations were summed to the intensity of the primary fragment.

Infrared multiphoton dissociation (IRMPD) spectra were collected with a Bruker Esquire 3000 IT-MS mounted to a beamline of the free electron laser CLIO (Centre Laser Infrarouge Orsay, Orsay, France).[14] For the IRMPD measurements the ions of interest were mass selected and stored within the ion trap prior to admittance of several laser macropulses inducing fragmentation. The measure of relative abundances of the parent and fragment ions as a function of the photon energy provided the experimental IRMPD spectra.[15]

The theoretical calculations were performed using the mPW1PW91[16] density functional in conjunction with LanL2DZ basis set for gold and cc-pVDZ basis set for the remaining elements as implemented in the Gaussian 09 program package.[17] All of the calculations included complete geometry optimization, as well as calculation of the Hessian matrix, that confirmed the nature of all stationary points and afforded zero-point energy (ZPE) corrections and theoretical IR spectra. Reported energies refer to a temperature 0 K in the gas phase. The predicted gas phase IR spectra were convoluted with a Gaussian function with a full width at half-maximum (fwhm) of 20 cm^{-1}. The computed frequencies were scaled by a factor of 0.965 to obtain optimal match between the experimental IRMPD and theoretical spectra.[18,19]

RESULTS AND DISCUSSION

Gold(I) α-oxo carbenes constitute a remarkable class of highly reactive intermediates that may be generated in situ by catalytic oxidation of alkynes and trapped in various ways. However, no direct experimental evidence for their involvement or their formation in gold catalyzed oxidation reaction has been obtained so far. Hence, we decided to study the possible formation of gold(I) α-oxo carbenes supported by the ancillary ligand IPr (IPr = 1,3-bis(2,6-diisopropylphenyl)imidazol-2-ylidene) by using electrospray ionization mass spectrometry. If these elusive species are stable on the order of milliseconds it should be possible to transfer them to the gas phase and probe their structure. To this end we selected a group of cognate internal as well as terminal alkynes, namely, 1-phenylpropyne, 2-butyne, diphenylacetylene and phenylacetylene, and probed the gold(I) complexes formed in the oxidation reaction.

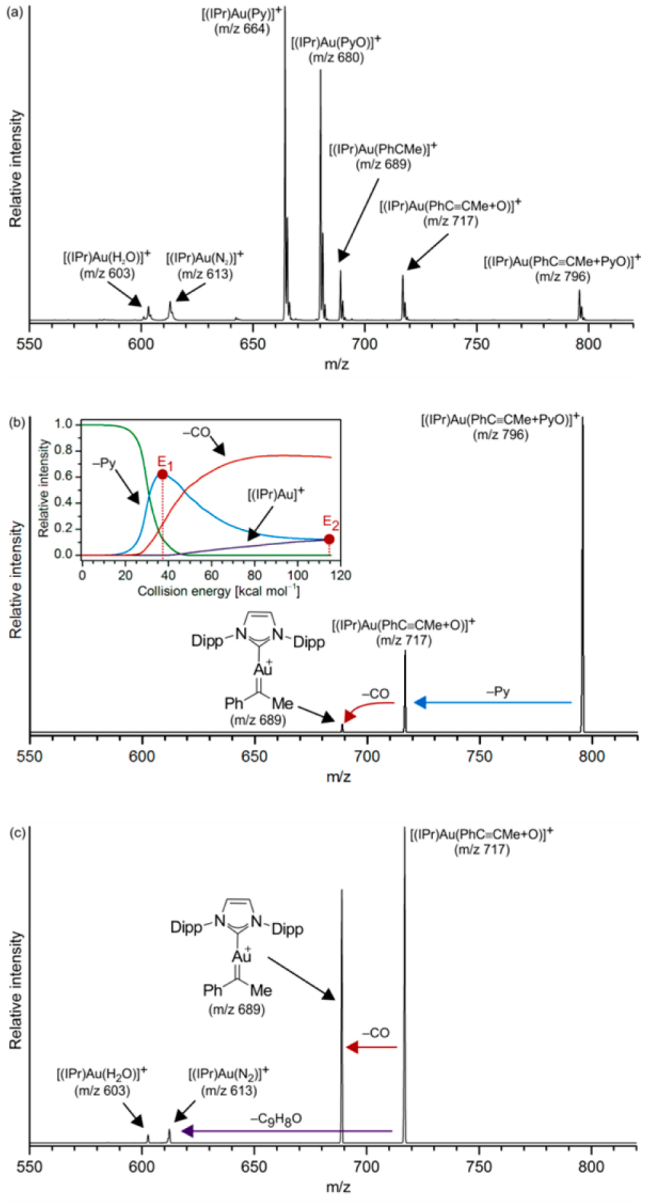

Figure 1. (a) Section of the ESI-MS source spectrum of dichloromethane solution of 1-phenylpropyne, pyridine *N*-oxide and gold(I) complex [(IPr)Au(CH_3CN)][BF4]. (b) Section of the daughter-ion mass spectra of [(IPr)Au(PhC≡CMe+PyO)]$^+$ and the corresponding energy-resolved CID (inset). The collision energies E_1 and E_2 were used to generate ions [(IPr)Au(PhC≡CMe+O)]$^+$ for MS^3 energy-resolved CID experiments (cf. Figure 2). (c) Section of the MS^3 daughter-ion mass spectra of [(IPr)Au(PhC≡CMe+O)]$^+$ generated from precursor ions with collision energy E_2. Dipp = 2,6-diisopropylphenyl.

Energy-Resolved CID Experiments. First, we have probed the possibility to generate gold(I) α-oxo carbenes by electrospray ionization and consequently the species of interest were subjected to collision-induced dissociation (CID) experiments. The ions were obtained by electrospray ionization from dichloromethane solution of respective alkyne, pyridine *N*-oxide (PyO) and gold(I) complex [(IPr)Au(CH_3CN)][BF_4].

A representative mass spectrum of a reaction mixture (Figure 1a, alkyne = 1-phenylpropyne) shows that we can detect ions

dx.doi.org/10.1021/ja505945d | J. Am. Chem. Soc. 2014, 136, 11513−11523

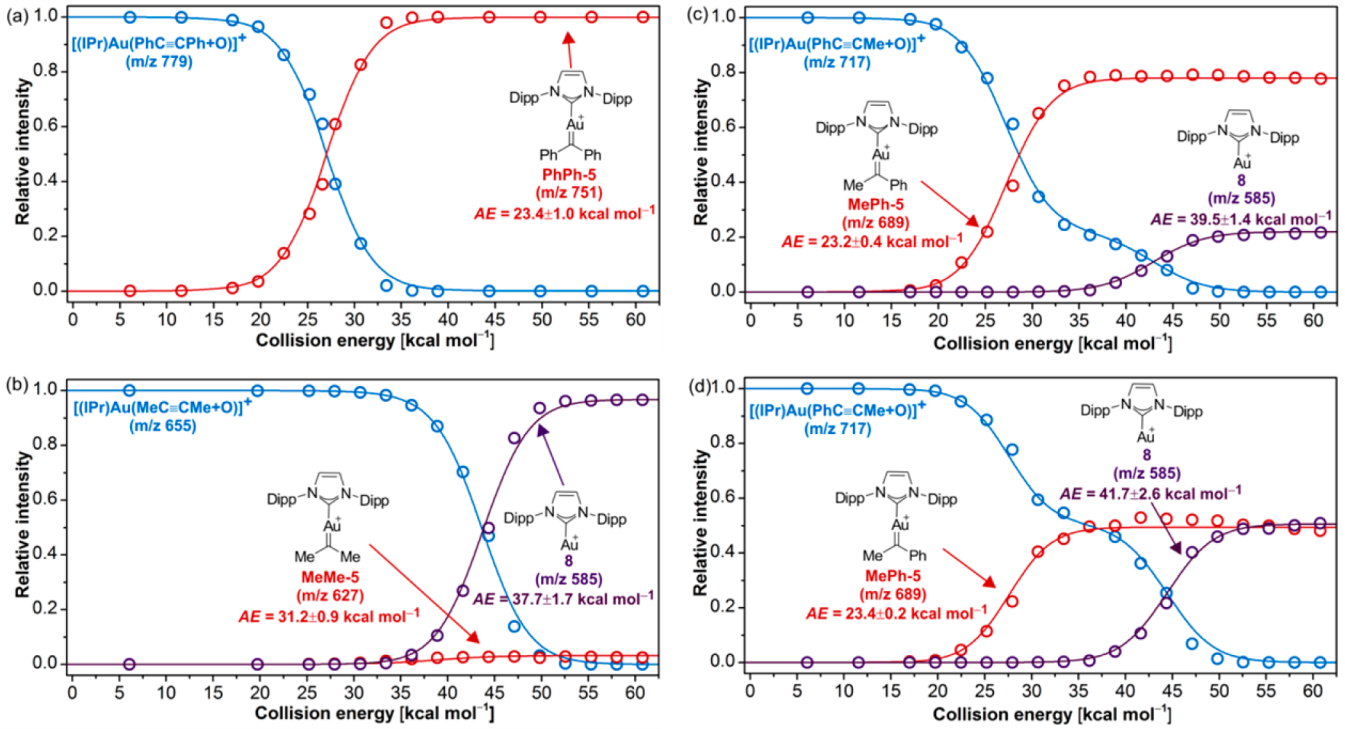

Figure 2. MS^3 energy-resolved CID (symbols) of the ions $[(IPr)Au(R^1C{\equiv}CR^2{+}O)]^+$ where R^1/R^2 = Ph/Ph (a), Me/Me (b) or Me/Ph (c,d). Dipp = 2,6-diisopropylphenyl. The parent-ions were generated from $[(IPr)Au(PhC{\equiv}CMe{+}PyO)]^+$ precursors using collision energy E_1 (ca. 40 kcal mol^{-1}, c) or E_2 (ca. 120 kcal mol^{-1}, d) (cf. Figure 1).

corresponding to the addition of pyridine *N*-oxide to the gold-activated alkyne ($[(IPr)Au(R^1C{\equiv}CR^2{+}PyO)]^+$) as well as the ions corresponding to a subsequent elimination of pyridine ($[(IPr)Au(R^1C{\equiv}CR^2{+}O)]^+$). Tentatively, we have assigned these species as β-gold(I) vinyloxypyridinium complexes and gold(I) α-oxo carbenes, respectively. Next, we can also observe formation of carbene complexes $[(IPr)Au(R^1CR^2)]^+$, which are most probably formed in CID processes during the transfer of the ions to the mass analyzer (see below the CID experiments).[20]

Collision-induced dissociation experiments with mass-selected ions confirmed that the parent species $[(IPr)Au(R^1C{\equiv}CR^2{+}PyO)]^+$ afford the putative gold(I) α-oxo carbenes $[(IPr)Au(R^1C{\equiv}CR^2{+}O)]^+$ by elimination of pyridine (Figure 1b and Figure S2 in the Supporting Information). Elimination of pyridine can be followed by expulsion of CO or by releasing of the $[(IPr)Au]^+$ cation. The inset in Figure 1b shows dependence of abundance of different fragmentation channels on the collision energy.

The gold(I) α-oxo carbenes generated by CID of $[(IPr)Au(R^1C{\equiv}CR^2{+}PyO)]^+$ were again mass-selected and subjected to the next CID experiment (the MS^3 energy-resolved CID experiments performed on mass-selected $[(IPr)Au(R^1C{\equiv}CR^2{+}O)]^+$ ions generated by fragmentation of the precursor ions $[(IPr)Au(R^1C{\equiv}CR^2{+}PyO)]^+$ (Figure 2a–d)). The branching ratios between the CO elimination and the $[(IPr)Au]^+$ liberation strongly depend on the substituents of the CC triple bond of the oxidized alkyne (R^1 and R^2 in Scheme 2). If both substituents are aromatic (i.e., phenyl groups), then the CO loss represents the exclusive fragmentation channel (Figure 2a). On the contrary, if both substituents are aliphatic (i.e., methyl groups) then the liberation of the $[(IPr)Au]^+$ ion strongly prevails (Figure 2b). For the alkyne bearing one phenyl group and one methyl group both fragmentation channels are observed. Interestingly, the branching ratio between the two fragmentation channels depends on the collision energy with which the parent ions $[(IPr)Au(PhC{\equiv}CMe{+}O)]^+$ are generated from the precursors $[(IPr)Au(PhC{\equiv}CMe{+}PyO)]^+$. If the $[(IPr)Au(PhC{\equiv}CMe{+}O)]^+$ ions are generated with a lower collision energy, then the elimination of carbon monoxide prevails ($E_1 \sim$ 40 kcal mol^{-1}, Figure 2c), whereas the generation of $[(IPr)Au(PhC{\equiv}CMe{+}O)]^+$ by using high collision energies ($E_2 \sim$ 120 kcal mol^{-1}, Figure 2d) leads to a comparable abundance of both channels.

The relative abundances of the daughter-ions formed upon CID of $[(IPr)Au(PhC{\equiv}CMe{+}O)]^+$ were not only changing as a function of energy with which the parent ions were generated, but also as a function of reaction time. To demonstrate this behavior we have performed an experiment in which we monitored the relative abundances of the daughter-ions formed upon MS^3 CID of $[(IPr)Au(PhC{\equiv}CMe{+}O)]^+$ as a function of reaction time, while the collision energies used to form the parent-ions $[(IPr)Au(PhC{\equiv}CMe{+}O)]^+$ from the precursor-ions ($E_1 \sim$ 40 kcal mol^{-1}) and to dissociate them ($E_{coll} \sim$ 30 kcal mol^{-1}) were kept constant. The relative abundances of the daughter-ions changed during the experiment so that the abundance of carbon monoxide elimination channel was slowly decreasing (Figure 3). This behavior was even more pronounced when using higher collision energy for generation of parent-ions $[(IPr)Au(PhC{\equiv}CMe{+}O)]^+$ ($E_2 \sim$ 120 kcal mol^{-1}, see Figure S4 in the Supporting Information). As a result the initially minor fragmentation channel (i.e., releasing of $[(IPr)Au]^+$) prevailed in the CID experiment after ca. 90 min. These findings strongly suggests that two different isomers of the parent ions $[(IPr)Au(PhC{\equiv}CMe{+}O)]^+$ are formed, and their formation depends on the substituents of the CC triple bond in the $[(IPr)Au(R^1C{\equiv}CR^2{+}PyO)]^+$ precursors.

dx.doi.org/10.1021/ja505945d | J. Am. Chem. Soc. 2014, 136, 11513–11523

Scheme 2. Collision-Induced Dissociation (CID) Reactions Observed for Ions $[(IPr)Au(R^1C{\equiv}CR^2{+}PyO)]^+$ and $[(IPr)Au(R^1C{\equiv}CR^2{+}O)]^+$

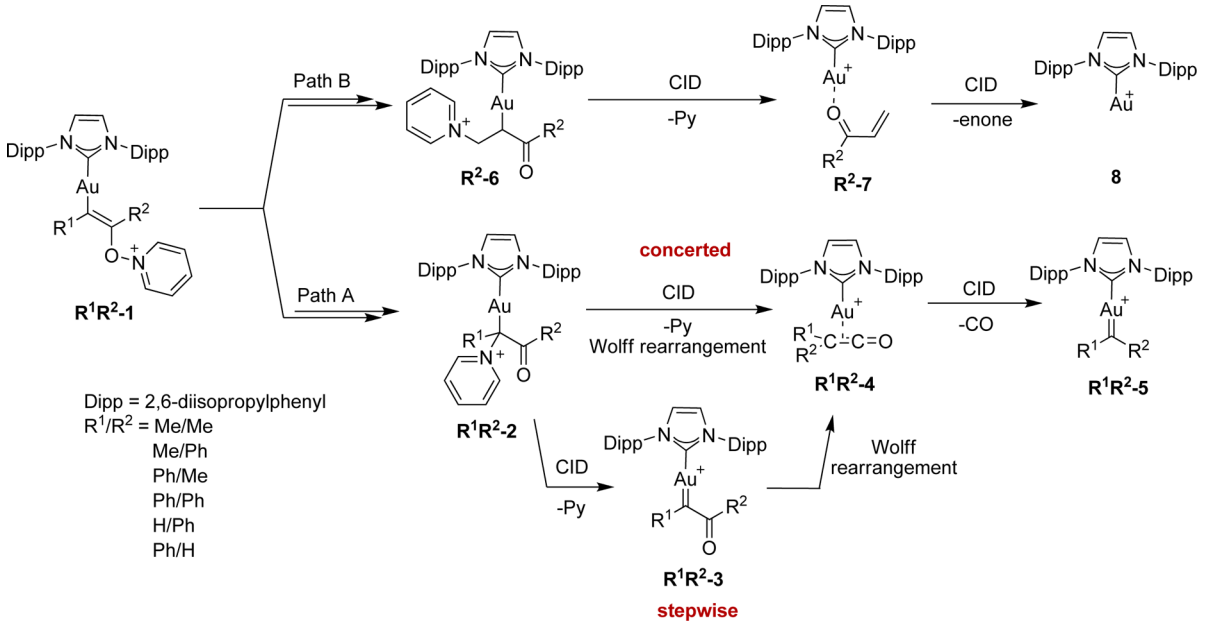

We have also tested the formation of the putative intermediates in the oxidation of phenylacetylene (terminal alkyne). The precursor ions $[(IPr)Au(PhC{\equiv}CH{+}PyO)]^+$ (m/z 782) can be generated, but the subsequent elimination of pyridine is immediately followed by the CO expulsion (see Figure S2 in the Supporting Information). We can also observe a small abundance of the $[(IPr)Au]^+$ liberation, but it stays negligible at all collision energies used.

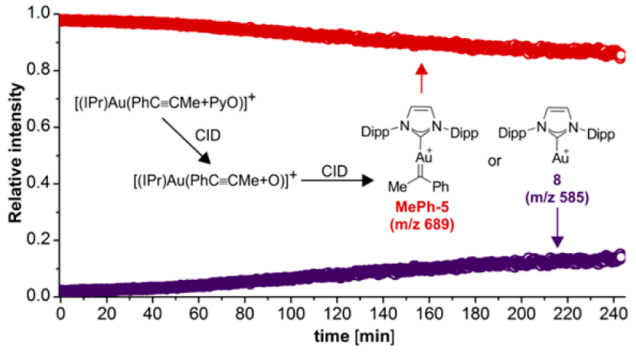

Figure 3. Time dependence of the relative abundances of the daughter-ions formed upon MS^3 CID of species $[(IPr)Au(PhC{\equiv}CMe{+}O)]^+$. Collision energies were constant (E_1 = 40 kcal mol^{-1}, E_{coll} = 30 kcal mol^{-1}, see the text). Dipp = 2,6-diisopropylphenyl.

The energy-resolved CID experiments allow us to determine the appearance energies for the individual channels (Figure 2). At the first sight, it is clear that the decarbonylation channel appears at a lower activation energy (~20 kcal mol^{-1}) than the $[(IPr)Au]^+$ liberation (~40 kcal mol^{-1}), and the activation energies for the two channels depend only slightly on the substitution of the alkyne reactant.

The performed experiments clearly suggest that we are dealing with two possible isomeric structures. There are numerous possible isomers that can be suggested to be formed next to the putative α-oxo carbene moiety (Scheme 3). For example, gold(I) α-oxo carbenes are frequently viewed as synthetic surrogates α-diazocarbonyl compounds, that in turn are generally known to undergo the Wolff rearrangement yielding ketenes.[21] Ketenes can easily undergo the CO elimination under various conditions including activation by a transition metal.[22] Hence, the facile decarbonylation of the complexes studied here could be explained by the rearrangement of α-oxo carbenes to ketenes. It should be, however, pointed out that α-oxo carbenes are prone to diverse rearrangements affording a variety of isomers that can be even mutually convertible.[23] The plausible isomers taken into account in this work are summarized in Scheme 3.

Scheme 3. Plausible Structures of Ionic Species $[(IPr)Au(R^1C{\equiv}CR^2{+}O)]^+$

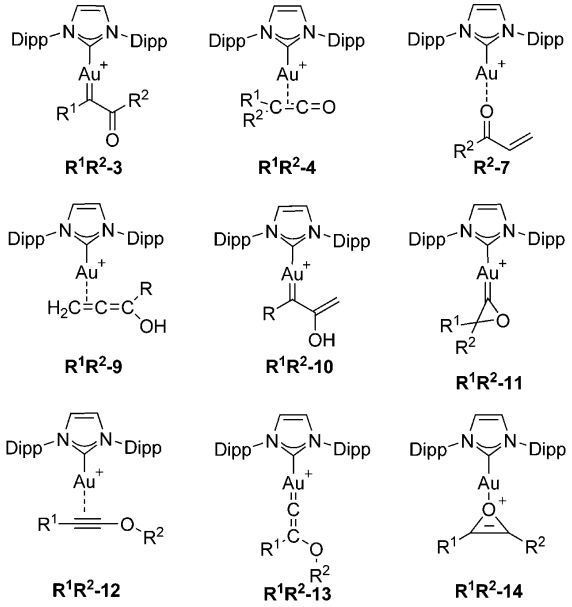

Infrared Multiphoton Dissociation (IRMPD) Spectroscopy. The most straightforward strategy to disentangle the

dx.doi.org/10.1021/ja505945d | J. Am. Chem. Soc. 2014, 136, 11513−11523

possible structures of the generated complexes is to apply infrared multiphoton dissociation spectroscopy (IRMPD).[24] The obtained infrared spectral characteristics of the gaseous ions can be then assigned to the particular ionic structures based on theoretical calculations.[25]

We have focused on the ionic complexes generated from the oxidation reaction of 1-phenylpropyne as potentially both isomers of gold-containing intermediates could be present. The IRMPD spectrum of $[(IPr)Au(PhC{\equiv}CMe{+}PyO)]^+$ is shown in Figure 4a along with the calculated gas phase IR spectra of selected plausible ionic structures (Figure 4b–f).

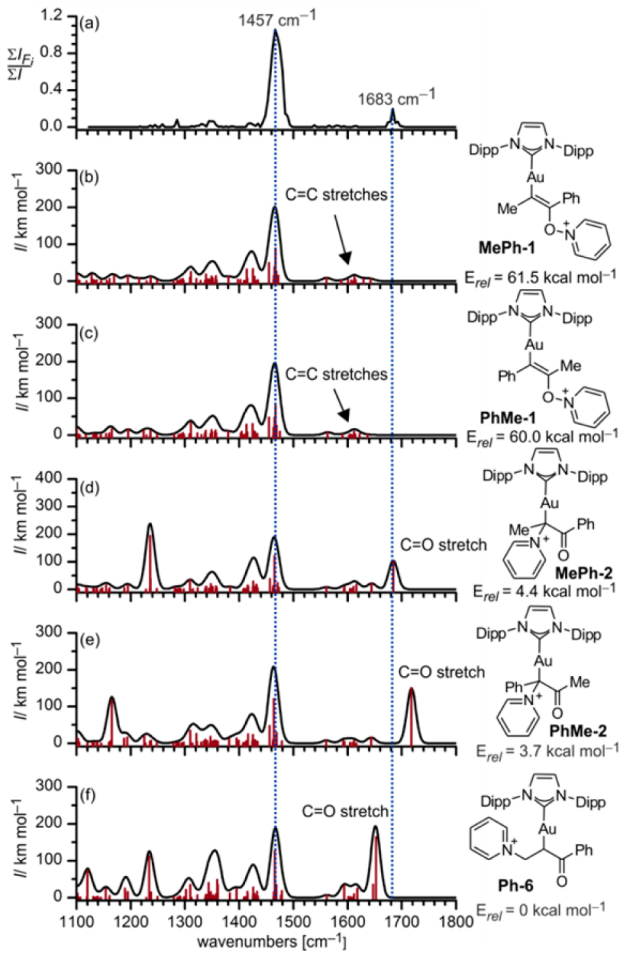

Figure 4. Experimental IRMPD spectrum of $[(IPr)Au(PhC{\equiv}CMe{+}PyO)]^+$ (m/z 796) (a) and theoretical gas phase IR spectra of conceived candidates calculated at mPW1PW91/cc-pVDZ:LanL2DZ-(Au) level of theory (b–f). The scaling factor of 0.965 was used for the computed wavenumbers.

The experimental IRMPD spectrum of $[(IPr)Au(PhC{\equiv}CMe{+}PyO)]^+$ displays two major bands. On the basis of the comparison with the predicted IR spectra we attributed the dominant band at 1467 cm^{-1} to composite vibrations mainly due to the stretching modes of ancillary ligand IPr. The second band at 1683 cm^{-1} occurs in the spectral range typical for the stretching vibrations of double bonds. There are no bands around 1683 cm^{-1} in the theoretical IR spectra of two possible β-gold(I) vinyloxypyridinium isomers **MePh-1** and **PhMe-1**. All C═C stretches in **MePh-1** and **PhMe-1** are found at considerably lower wavenumbers.

Hence, the primary product of pyridine *N*-oxide addition to 1-phenylpropyne is not transferred to the gas phase, and instead we detect a product of a rearrangement. The obvious possibility is a migration of the pyridine unit to the neighboring carbon atom. The C═O vibration of the so formed α-oxo carbenoids **MePh-2** and **PhMe-2** matches the experimental wavenumbers quite well. The rearrangement of the primary pyridine *N*-oxide adducts to the α-oxo carbenoids **2** is exothermic by almost 60 kcal mol^{-1}. We have considered also other possible isomers of $[(IPr)Au(PhC{\equiv}CMe{+}PyO)]^+$, but none of them yielded a theoretical spectrum that would be in agreement with the experimental spectrum (see Figure S6 in the Supporting Information). Comparison of the theoretical IR spectra of **MePh-2** and **PhMe-2** with the experiment suggests the less stable isomer **MePh-2** is most probably formed. It can be rationalized based on the primary attack of pyridine *N*-oxide at the more stable carbocationic site of the gold-activated alkyne (Markovnikov rule).[26] Hence, oxygen atom is transferred to the carbon atom neighboring the phenyl group rather than that neighboring the methyl group. The precursor ions thus most probably correspond to carbenoids **MePh-2**, but we will consider both isomers in the following discussion. The elimination of pyridine should lead to the gold(I) α-oxo carbenes **MePh-3** and **PhMe-3**, but it can also promote some rearrangements. The gas phase structure of $[(IPr)Au(PhC{\equiv}CMe{+}O)]^+$ generated in the MS/MS experiment from $[(IPr)Au(PhC{\equiv}CMe{+}PyO)]^+$ was therefore again probed by IRMPD spectroscopy. We have plotted separately the spectra obtained by monitoring of the CO elimination (Figure 5a) and of the $[(IPr)Au]^+$ liberation (see Figure S7 in the Supporting Information).

The spectrum obtained for the CO elimination channel contains two intense bands at 1469 and 2155 cm^{-1}. The liberation of $[(IPr)Au]^+$ was only very weakly populated, and therefore the corresponding IRMPD spectrum has very low intensity. Nevertheless, the spectrum clearly contains one more band at about 1575 cm^{-1}. Comparison of the IRMPD spectra with the theoretical IR spectra undoubtedly reveals that the generated $[(IPr)Au(PhC{\equiv}CMe{+}O)]^+$ species do not correspond the gold(I) α-oxo carbenes **MePh-3** and **PhMe-3** (Figure 5b,c). Instead, the intense band at 2155 cm^{-1} suggests that the Wolff rearrangement to the corresponding ketene took place. Accordingly, the theoretical spectrum of the corresponding gold(I) ketene complex **MePh-4a** (Figure 5d) is in a very good agreement with the experimental spectrum obtained for the CO elimination. The spectral band at 1469 cm^{-1} is attributed to the convolution of vibrational modes of the ancillary ligand IPr and the band at 2155 cm^{-1} corresponds to the stretching mode of the ketene moiety. We note in passing that a favorable match of the experimental and theoretical spectra can be found also for gold(I) phenyl 1-propynyl ether complex **MePh-12** (Figure 5e), but the rearrangement to the ketene complex is thermodynamically as well as kinetically favored and therefore also more probable (see Figure S15 in the Supporting Information).

As the IRMPD spectrum obtained for the $[(IPr)Au]^+$ liberation is very weak and does not correspond to any of the first-hand structures, we have decided to investigate IRMPD spectra of the gold complexes obtained from the oxidation mixture with 2-butyne. Although the IRMPD spectrum of $[(IPr)Au(MeC{\equiv}CMe{+}PyO)]^+$ (Figure 6a) is virtually the same as that of $[(IPr)Au(PhC{\equiv}CMe{+}PyO)]^+$ (see above), agreement between the predicted IR spectrum of corresponding carbenoid **MeMe-2** (Figure 6c) and the experimental spectrum is not satisfactory. Hence, we have considered the possible

dx.doi.org/10.1021/ja505945d | J. Am. Chem. Soc. 2014, 136, 11513–11523

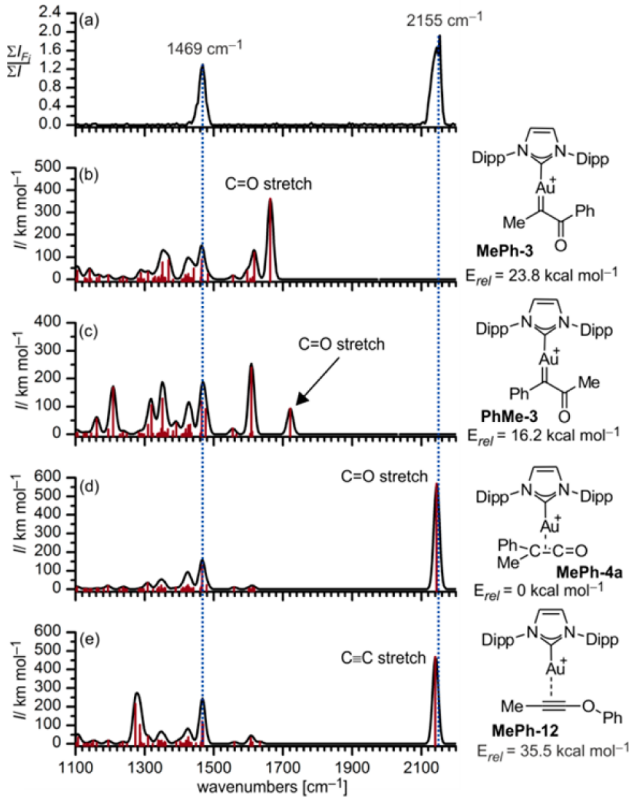

Figure 5. Experimental IRMPD spectrum of $[(IPr)Au(PhC{\equiv}CMe+O)]^+$ (m/z 717) generated by CID from $[(IPr)Au(PhC{\equiv}CMe+PyO)]^+$ (a) and predicted IR spectra of possible ion structures in the gas phase calculated at mPW1PW91/cc-pVDZ:LanL2DZ(Au) level of theory (b–e). The scaling factor of 0.965 was used for the computed wavenumbers.

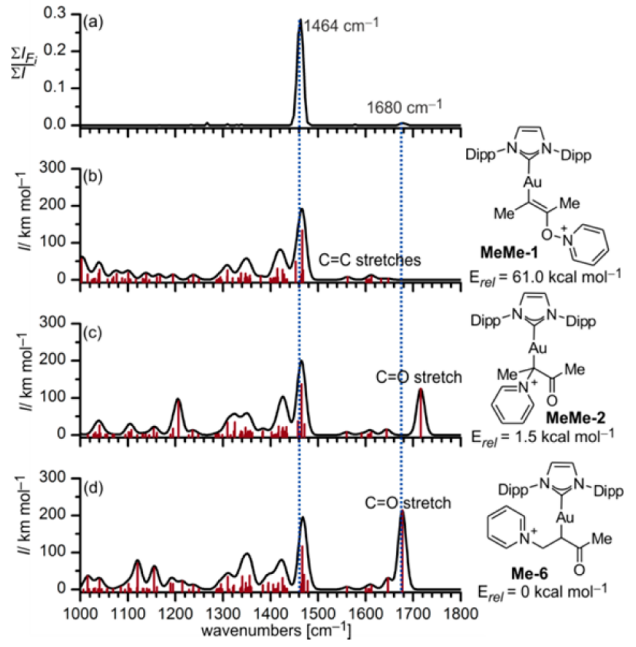

Figure 6. Experimental IRMPD spectrum (a) of $[(IPr)Au(MeC{\equiv}CMe+PyO)]^+$ (m/z 734) and predicted IR spectra of possible ion structures in the gas phase calculated at mPW1PW91/cc-pVDZ:LanL2DZ(Au) level of theory (b–d). The scaling factor of 0.965 was used for the computed wavenumbers.

formation of another pyridinium adducts. The best agreement was achieved when we considered that the primary pyridine *N*-oxide undergoes a hydrogen rearrangement from the methyl group to the neighboring carbon atom (Scheme 2). This rearrangement would be associated with a formation of adduct **Me-6** between a gold complex of 2-butenone and pyridine. The predicted IR spectrum of **Me-6** (Figure 6d) is in the best accordance with the IRMPD spectrum of $[(IPr)Au(MeC{\equiv}CMe+PyO)]^+$ from all isomers considered. It suggests that not only the ionic structures of putative gold(I) α-oxo carbenes but also the precursor ions $[(IPr)Au(R^1C{\equiv}CR^2{+}PyO)]^+$ can be thus present as different isomers.

The prevailing ionic fragment formed upon CID of $[(IPr)Au(MeC{\equiv}CMe{+}O)]^+$ corresponds to $[(IPr)Au]^+$. The same fragmentation was observed during measurement of the IRMPD spectrum (Figure 7a). Comparison of the experimental spectrum

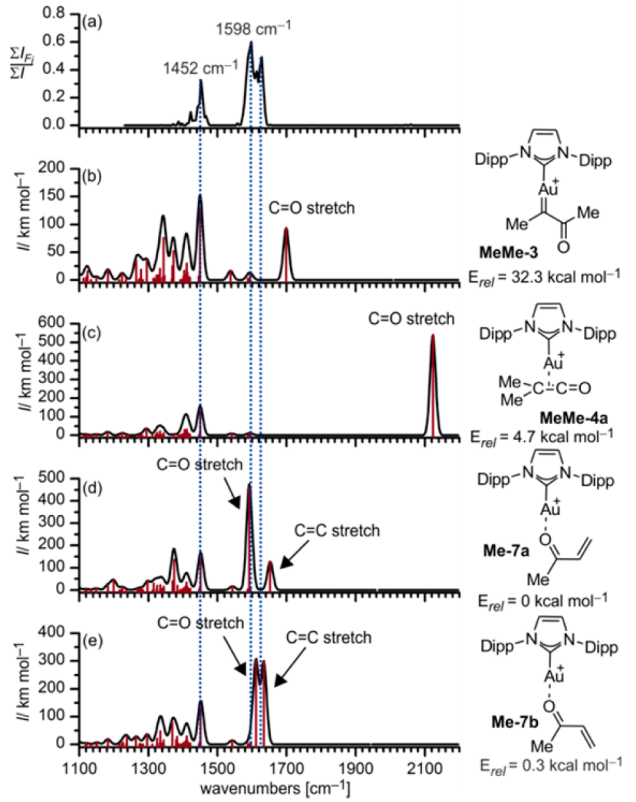

Figure 7. Experimental IRMPD spectrum (a) of $[(IPr)Au(MeC{\equiv}CMe+O)]^+$ (m/z 655) generated by CID from $[(IPr)Au(MeC{\equiv}CMe+PyO)]^+$ and predicted IR spectra of possible ion structures in the gas phase calculated at mPW1PW91/cc-pVDZ:LanL2DZ(Au) level of theory (b–e). The scaling factor of 0.955 was used for the computed wavenumbers.

of $[(IPr)Au(MeC{\equiv}CMe{+}O)]^+$ with theoretical IR spectra of plausible isomeric structures reveals that neither gold(I) α-oxo carbene **MeMe-3** (Figure 7b) nor ketene complex **MeMe-4a** (Figure 7c) can account for the observed spectral bands. The obvious alternative is a complex of 2-butenone formed by the elimination of pyridine from **Me-6** (see above). The gold cation is preferentially coordinated to the oxygen atom. Coordination to the CC double bond leads to isomeric complexes lying of about 6 kcal mol^{-1} higher in energy. The mutual orientation of the double bonds can be either cisoid (**Me-7a**) or transoid (**Me-7b**), the former being favored by 0.3 kcal mol^{-1}. Comparison of

dx.doi.org/10.1021/ja505945d | J. Am. Chem. Soc. 2014, 136, 11513–11523

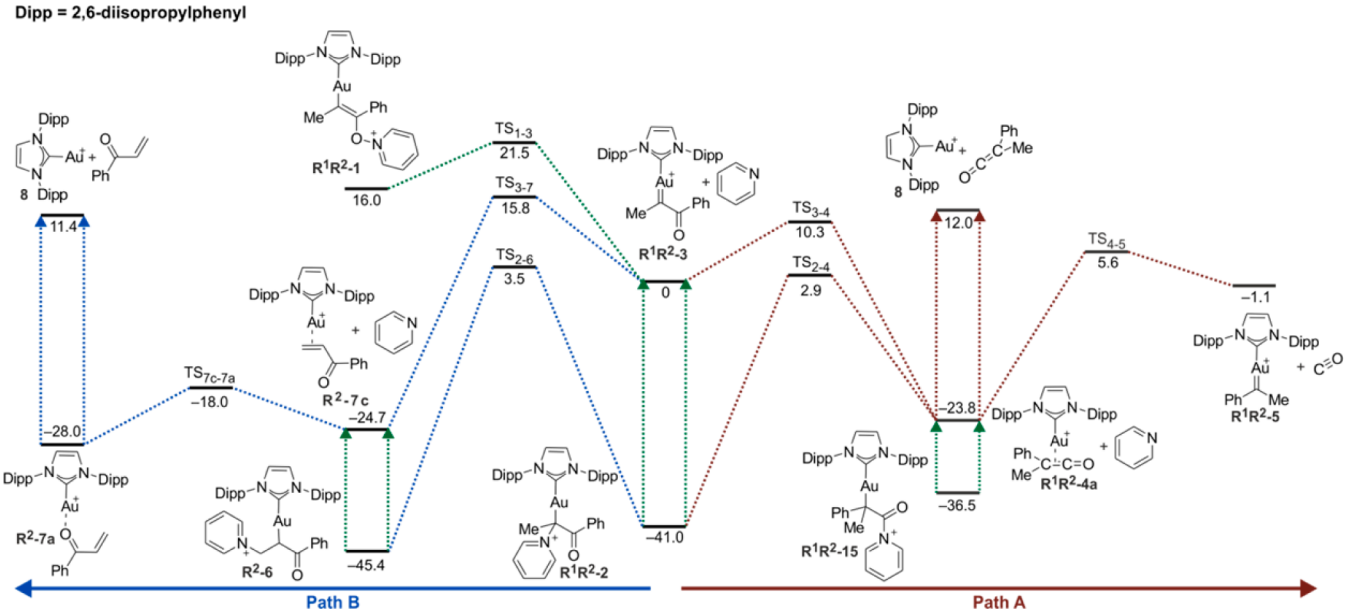

Figure 8. Schematic representation of the potential energy surface for the formation and proposed rearrangements of putative gold(I) α-oxo carbenes **MePh-3**; i.e., R^1 = Me and R^2 = Ph. Relative energies calculated at the mPW1PW91/cc-pVDZ:LanL2DZ(Au) level of theory (kcal mol^{-1}, including zero-point energy corrections).

Table 1. Relative Energies for the Formation of Gold(I) α-Carbenes R^1R^2-3 and Following Rearrangements into Corresponding Ketene and Enone Complexes Calculated at the mPW1PW91/cc-pVDZ:LanL2DZ(Au) Level of Theory (kcal mol^{-1}, Including Zero-Point Energy Corrections)

	R^1R^2-X					
X	MeMe-X	MePh-X	PhMe-X[a]	PhPh-X	HPh-X	PhH-X[b]
1	12.9	16.0	14.6	25.6	7.1	9.4
2	−46.6	−41.0	−41.7	−30.4	−57.4	−46.9
TS_{1-3}	18.3	21.5	20.8	32.2	15.6	14.9
3+Py	0	0	−7.6	0	0	−6.5
TS_{2-4}	1.9	2.9	2.8	9.2	−5.2	−6.1
TS_{3-4}	9.4	10.3	8.6	15.7	10.6	1.1
15	−39.0	−36.5	−36.5	−26.9	−49.5	−49.5
4a+Py	−27.7	−23.8	−23.8	−13.1	−34.5	−34.5
TS_{4-5}	5.5	5.6	5.6	15.9	−1.6	−1.6
5+CO	3.5	−1.1	−1.1	4.9	−4.2	−4.2
8+ketene	10.5	12.0	12.0	22.2	2.0	2.0
TS_{2-6}	1.9	3.5	–	–	–	–
6a	−48.1	−45.4	–	–	–	–
TS_{3-7}	14.1	15.8	–	–	–	–
7c+Py	−26.4	−24.4	–	–	–	–
TS_{7c-7a}	−18.5	−18.0	–	–	–	–
7a	−32.3	−28.0	–	–	–	–
8+enone	7.8	11.4	–	–	–	–

[a] *ZPE*-corrected energies given relative to (**MePh-3**+Py). [b] *ZPE*-corrected energies given relative to (**HPh-3**+Py).

the IRMPD spectrum of $[(IPr)Au(MeC{\equiv}CMe{+}O)]^+$ and theoretical IR spectra of **Me-7a** and **Me-7b** allows us to assign the composite band in the region between 1560 and 1650 cm^{-1} as stretching modes of CC and CO double bonds. The intensity and three maxima of the experimental band suggest that both conformers (cisoid and transoid) are present in the ionic mixture.

Density Functional Theory Calculations. With the aim to provide further insight into the nature and energetics of the observed rearrangements and fragmentations of the species under the study we have performed DFT calculations at the mPW1PW91/cc-pVDZ:LanL2DZ(Au) level of theory. Figure 8 shows schematic representation of the potential energy surface for the formation of gold(I) α-oxo carbenes **MePh-3** and following rearrangements leading to corresponding isomeric structures revealed by the IRMPD experiments. Table 1 summarizes the corresponding relative energies calculated for the remaining systems under study.

The predicted potential energy surface shows that the formation of gold(I) α-oxo carbenes R^1R^2-**3** from β-gold(I) vinyloxypyridinium complexes R^1R^2-**1** is exothermic with the activation barriers of only 5.4−8.5 kcal mol^{-1}. On the contrary, the formations of adducts R^1R^2-**2** between pyridine and the respective gold(I) α-oxo carbenes is highly exothermic with bond dissociation energies (BDE) ranging from 30.4 to 57.4 kcal

dx.doi.org/10.1021/ja505945d | J. Am. Chem. Soc. 2014, 136, 11513−11523

mol^{-1}. Hence, it is very probable the β-gold(I) vinyloxypyridinium complexes will easily lose the pyridine molecule at the laboratory temperature, and the primarily formed gold(I) α-oxo carbenes will immediately again associate with pyridine to form the carbenoid complex $\mathbf{R^1R^2}$**-2**. We have searched for a transition structure for a rearrangement of the pyridine unit from the oxygen atom to the carbon atom in one step, but we could not have localized it. With respect to the role of β-gold(I) vinyloxypyridinium ions it is important to note that their energy as well as the energy necessary for their fragmentation is higher than all other stationary points on the considered potential energy surface. Hence, if such ions would be transferred to the gas phase, we would never be able to detect the products of pyridine elimination, but we would immediately observe subsequent fragmentations. On the basis of the experiments we can thus exclude that these complexes are transferred to the gas phase.

The elimination of pyridine from $\mathbf{R^1R^2}$**-2** leads back to the gold(I) α-oxo carbenes that can either undergo a Wolff rearrangement to form the corresponding ketene (Path A in Figure 8) or a hydrogen atom can migrate to the carbene carbon atom from the neighboring carbon atom (Path B). The energy demands for the Wolff rearrangement (TS_{3-4}) depend on the substitution. Hence, for the dimethyl substituted α-oxo carbenes (R^1 = R^2 = Me) it amounts to 9.4 kcal mol^{-1}, whereas the migration of the phenyl group in the diphenyl substituted species is associated with the energy barrier of 15.7 kcal mol^{-1}. For the methyl, phenyl substituted α-oxo carbenes, the barrier heights for the migration of either group is largely influenced by the relative stability of the parent ions. Hence, if the carbene-carbon atom bears the phenyl group, the carbene is more stable and the migration of the methyl group leads over an energy barrier of 16.2 kcal mol^{-1}. On the other hand, the α-oxo carbene bearing the methyl group at the carbene-carbon atom is less stable and consequently, the migration of the phenyl group to form the ketene product is associated with an energy barrier of only 10.3 kcal mol^{-1}. The barriers can be even smaller, if we consider that the elimination of pyridine from the carbenoids is already associated with the Wolff rearrangement (TS2−4). The overall energy barriers are lowered by 6−7 kcal mol^{-1}.

Coordination of the $[(IPr)Au]^+$ cation to the ketenes can proceed at several sites. Typically, the η^2-coordination at either CC or CO double bond has been observed in ketene transition metal complexes.[27,28] From our theoretical calculations emerges that the cationic gold fragment $[(IPr)Au]^+$ prefers η^1-bonding modes with the ketene coordinated via the C2 carbon atom ($\mathbf{R^1R^2}$**-4a**). The coordination via the oxygen atom ($\mathbf{R^1R^2}$**-4b**) leads to complexes lying more than 10 kcal mol^{-1} higher in energy. For the phenyl substituted species π-bound structures ($\mathbf{R^1R^2}$**-4c** and $\mathbf{R^1R^2}$**-4d**) have been also localized lying rather close in energy to the most stable C2-coordinated complex (Figure 9).[29] The IRMPD spectrum of $[(IPr)Au(PhC{\equiv}CMe+O)]^+$ matches the theoretical spectrum of the most stable complex **MePh-4a**, but we cannot exclude the presence of the phenyl-ring coordinated complexes (Figure S7 in the Supporting Information).

Specific situation is found for the oxidation of the terminal alkyne phenylacetylene. The oxidation is selective and proceeds at the internal carbon atom (isomers denoted as **HPh-X**). The energy barrier for the Wolff rearrangement of the gold(I) α-oxo carbenes **HPh-3** amounts to 10.6 kcal mol^{-1}, all the remaining steps are below the energy of the starting α-oxo carbene **HPh-3**. Consideration of the simultaneous Wolff rearrangement and

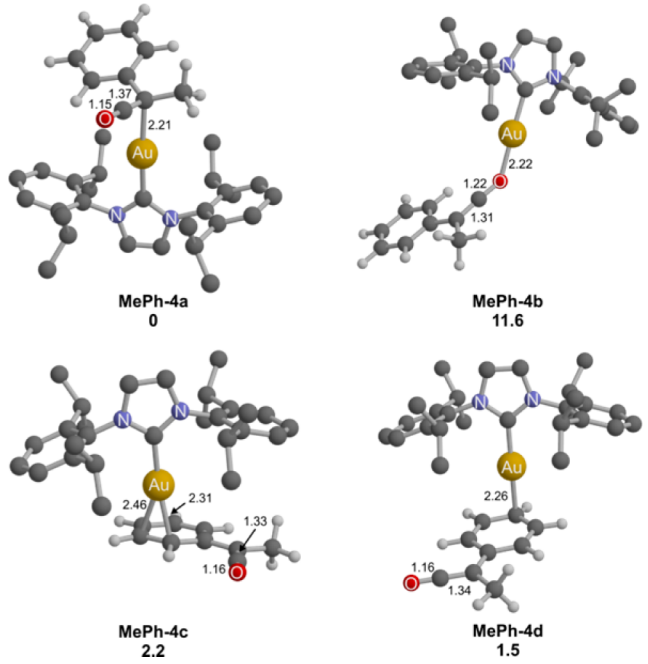

Figure 9. Structures of possible linkage isomers of gold(I) ketene complex **MePh-4** optimized at the mPW1PW91/cc-pVDZ:LanL2DZ-(Au) level of theory and relative ZPE-corrected energies (in kcal mol^{-1}) given to the most stable species. Selected bond lengths are given in Å. Only hydrogen atoms of ketene ligand are shown.

pyridine elimination leads to a drastic reduction of the barrier by about 16 kcal mol^{-1} and thus the whole reaction pathway toward elimination of CO lies below the energy of the α-oxo carbene **HPh-3**. It is in perfect agreement with the fact that it was not possible to detect the corresponding gold(I) α-oxo carbene generated from phenylacetylene in the experiment and only the product of decarbonylation was observed. We have considered also hypothetical oxidation at the terminal carbon atom of phenylacetylene (isomers denoted as **PhH-X**). The potential energy surface is analogous, but the migration of the hydrogen atom during the Wolff rearrangement is much more facile than the migration of the phenyl group as expected.

The concurrent reaction pathway (B in Figure 8) observed for alkyl substituted putative gold α-oxo carbenes **MeMe-3** and **PhMe-3** involves 1,2-H shift through the transition state $\mathbf{TS_{3-7}}$ to form the corresponding gold enone complexes ($\mathbf{R^2}$**-7**). Alternatively, enone complexes may be formed by a loss of pyridine from enone-adducts $\mathbf{R^2}$**-6**. The subsequent dissociation to the corresponding enone and $[(IPr)Au]^+$ is continuously endothermic process. From our calculations emerges that the gold(I) fragment $[(IPr)Au]^+$ prefers coordination to the carbonyl group over the coordination to the CC double bond of the enone molecule. The most stable isomers of gold(I) enone complexes $\mathbf{R^2}$**-7** correspond to the O-coordinated structures from which the cisoid forms are favored to the transoid forms. Figure 10 shows the optimized geometries of structures conceived for the complex **Me-7**.

Finally, we should rationalize the observed results in the CID experiments based on the obtained knowledge. The energy resolved CID experiments suggested that elimination of $[(IPr)Au]^+$ from all $[(IPr)Au(R^1C{\equiv}CR^2{+}O)]^+$ complexes is associated with about 40 kcal mol^{-1} activation energy. Dissociation of $\mathbf{R^2}$**-7** to the corresponding enone and $[(IPr)Au]^+$ amounts to 39.4 kcal mol^{-1} for R^2 = Ph and to 40.1 kcal mol^{-1} for

dx.doi.org/10.1021/ja505945d | J. Am. Chem. Soc. 2014, 136, 11513−11523

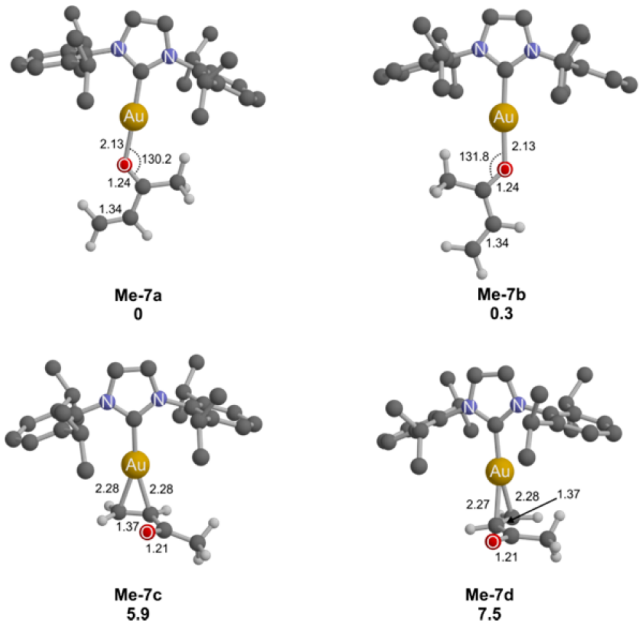

Figure 10. Isomeric structures of gold(I) enone complex **MeMe-7** optimized at the mPW1PW91/cc-pVDZ:LanL2DZ(Au) level of theory and relative ZPE-corrected energies (in kcal mol^{-1}) given to the most stable species. Only hydrogen atoms of enone ligand are shown.

R^2 = Me. Hence, it is in perfect agreement with the view that the elimination of $[(IPr)Au]^+$ originates from the enone complexes **R^2-7**, which are generated from their pyridine-adducts **R^2-6**. The experimental appearance energy for decarbonylation was determined as 23−31 kcal mol^{-1}. In theory, the elimination of CO from the gold complex of the corresponding ketene proceeds over the energy barriers of about 30 kcal mol^{-1} (**R^1R^2-4a** → **TS4−5**); hence, the theoretical energy barriers are slightly overestimated.

In the oxidation of 1-phenylpropyne, where both reaction pathways can be followed, the experimental results are consistent with the view that we are dealing originally with a mixture of ketene-gold complex and enone-gold complex. The relative changes in population of these two isomers generated from their pyridine adducts in the CID experiment (Figures 2cd) are caused by the fact that with the increasing collision energy, an increasing amount of the primarily generated ketene-gold complex undergoes immediate decarbonylation and is thus depleted from the mixture of $[(IPr)Au(PhC{\equiv}CMe{+}O)]^+$ complexes. The energy-dependent CID of the precursor ions $[(IPr)Au(PhC{\equiv}CMe{+}PyO)]^+$ suggest that the ketene-precursor ions, i.e., the gold(I) α-oxo carbenoids **MePh-2**, are far dominant ones. Nevertheless, aging of the reaction mixture leads to a progressive rearrangement of **MePh-2** to the more stable enone-adduct **Ph-6**, which is demonstrated by the changes of the CID pattern with the reaction time (cf. Figure 3).

Isotopic Labeling Experiments. The results of the experiments and DFT calculations suggest that the $[(IPr)Au(R^1C{\equiv}CR^2{+}PyO)]^+$ complexes do not correspond to the originally expected β-gold(I) vinyloxypyridinium complexes **R^1R^2-1**, but rather to gold(I) α-oxo carbenoid ions **R^1R^2-2** or to pyridine adducts of enones **R^2-7** (the **R^1R^2-2** are the dominant ones for R^1 = Me and R^2 = Ph—see above). The question remains, whether this observation is an artifact of electrospray ionization method or whether these complexes are really present also in the solution. Possible artifact of electrospray ionization may involve formation of the pyridine adducts during the spray process where large concentration gradients are involved.[30] This process would thus hinder us from detecting the elusive gold(I) α-oxo carbene ions. To check whether the ions $[(IPr)Au(R^1C{\equiv}CR^2{+}PyO)]^+$ are truly formed in a solution we have performed isotopic labeling study (Figure 11). First, the reaction mixture containing

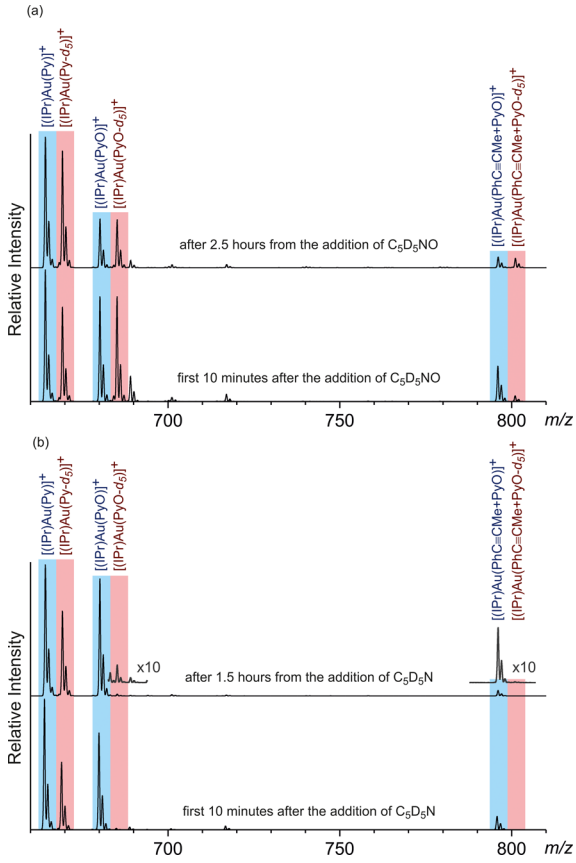

Figure 11. Time dependence of the relative abundances of the ions $[(IPr)Au(R^1C{\equiv}CR^2{+}PyO)]^+$ and $[(IPr)Au(R^1C{\equiv}CR^2{+}PyO\text{-}d_5)]^+$ upon addition of PyO-d_5 (a) and Py-d_5 (b) to a solution of 1-phenylpropyne, pyridine *N*-oxide and gold complex $[(IPr)Au(CH_3CN)][BF_4]$.

1-phenylpropyne (0.2 mmol), pyridine *N*-oxide (0.2 mmol) and the gold catalyst (1.0 μmol) in dichloromethane (1 mL) was allowed to react for 10 min. After initial reaction period D5-labeled pyridine *N*-oxide (0.2 mmol) was added and the reaction mixture was monitored for 2.5 h by ESI-MS. The performed experiment (Figure 11a) showed that the unlabeled species $[(IPr)Au(PhC{\equiv}CMe{+}PyO)]^+$ strongly prevails in the reaction mixture immediately after the addition of PyO-d_5 while the abundance of labeled ions $[(IPr)Au(PhC{\equiv}CMe{+}PyO\text{-}d_5)]^+$ gradually grows up until the complete equilibration after approximately 2 h. Clearly, if the pyridine adducts were formed during the electrospray ionization, the abundance of the unlabeled and the labeled complexes would be equal from the beginning of the experiment as observed, e.g., for labile complexes $[(IPr)Au(PyO)]^+$ and $[(IPr)Au(PyO\text{-}d_5)]^+$. The gradual equalization of the signals corresponding to the unlabeled and labeled carbenoids **R^1R^2-2** is due to their formation in the solution during the oxidation reaction.

In the next experiment, we wanted to check whether the pyridine-carbenoid complexes are formed in an intramolecular or

dx.doi.org/10.1021/ja505945d | J. Am. Chem. Soc. 2014, 136, 11513−11523

intermolecular reaction (i.e., whether the pyridine unit rearranges directly to the carbon atom, or whether the elusive gold(I) α-oxo carbene is formed, which then associates with another pyridine molecule). To this end, we have repeated the experiment in the same way but this time we added deuterium-labeled pyridine (0.2 μL) to the reaction mixture instead of PyO-d_5 (Figure 11b). Even though a significant amount of the gold complex $[(IPr)Au(Py\text{-}d_5)]^+$ was present in the reaction mixture immediately after the mixing we did not observe any formation of labeled ions $[(IPr)Au(PhC{\equiv}CMe{+}O{+}Py\text{-}d_5)]^+$. This observation supports the assumption that carbenoid complexes $\mathbf{R^1R^2}$**-2** are formed by a rearrangement of the β-gold(I) vinyloxypyridinium complexes $\mathbf{R^1R^2}$**-1** rather than via a capture of free gold(I) α-oxo carbenes $\mathbf{R^1R^2}$**-3**.

As the enone-complexes play only a minor role in the reaction of 1-phenylpropyne, we have repeated the labeling experiments also for the reaction with 2-butyne. The results are qualitatively the same; i.e., the pyridine adduct of butenone is formed already in the solution and there is no detectable exchange of the pyridine molecule in this adduct (Figure S10 in the Supporting Information). For the sake of completeness, the same experiments were also performed for the oxidation reaction of diphenylacetylene and phenylacetylene and the results are the same (Figure S11 and S12 in the Supporting Information).

CONCLUSIONS

We have used electrospray ionization mass spectrometry and infrared multiphoton dissociation spectroscopy to study the possible formation of gold(I) α-oxo carbenes in the intermolecular oxidation reactions of alkynes. From the performed experiments emerged that the initial β-gold(I) vinyloxypyridinium complexes **1** undergo a rearrangement to either gold(I) α-oxo carbenenoid **2** (a synthetic surrogate of the α-oxo carbene) or pyridine adduct of gold(I) enone complex **6** in the condensed phase. The latter reaction pathway can be followed, if the carbon atom neighboring with the hypothetical carbene−carbon atom bears a hydrogen atom. The isotopic labeling experiments strongly argue against the formation of free gold(I) α-oxo carbenes, because they show that (i) their pyridine adducts are transferred from the solution and not formed by an association upon the concentration changes during electrospray ionization and (ii) the carbenoids are formed most probably intramolecularly from the primarily formed β-gold(I) vinyloxypyridinium complexes.

If the gold(I) α-oxo carbenenoid **2** bears a methyl group at the carbene carbon atom, then a 1,2-H migration can occur leading to the more stable pyridine adduct of gold(I) enone complex **6**. This rearrangement is thermodynamically favored, and in accordance, time-resolved CID experiments demonstrated the growing concentration of **6** in the reaction mixture with time.

All the species involved in the reaction mechanism were unequivocally characterized by CID experiments and IRMPD spectroscopy. Using the labeling experiments, we have clearly linked the species isolated and characterized in the gas phase to the species existing in the condensed phase. Most importantly, we have shown the formation of the pyridinium adducts in the condensed phase and even their relative concentration changes during the aging of the reaction mixture. The pyridinium adducts can easily undergo nucleophilic substitution of pyridine in solution as well as in the gas phase; further work demonstrating this reactivity is in progress.

ASSOCIATED CONTENT

Supporting Information

Details on the experimental procedures and theoretical calculations, IRMPD spectra, potential energy surfaces, energies, optimized Gaussian geometries, and full ref 17. This material is available free of charge via the Internet at http://pubs.acs.org

AUTHOR INFORMATION

Corresponding Author

roithova@natur.cuni.cz

Notes

The authors declare no competing financial interest.

ACKNOWLEDGMENTS

Financial support from the European Research Council (StG ISORI) is gratefully acknowledged. The results from the CLIO were obtained owing to the founding from the European Union's Seventh Framework Programme (FP7/2007-2013) under the grant agreement No. 226716. The CLIO staff, particularly Philippe Maître and Vincent Steinmetz, are acknowledged for their help and assistance.

REFERENCES

(1) For selected general reviews aimed at gold catalysis, see: (a) Hashmi, A. S. K. *Chem. Rev.* **2007**, *107*, 3180−3211. (b) Fürstner, A.; Davies, P. W. *Angew. Chem., Int. Ed.* **2007**, *46*, 3410−3449. (c) Gorin, D. J.; Toste, F. D. *Nature* **2007**, *446*, 395−403. (d) Marion, N.; Nolan, S. P. *Chem. Soc. Rev.* **2008**, *37*, 1776−1782. (e) Li, Z.; Brouwer, C.; He, C. *Chem. Rev.* **2008**, *108*, 3239−3265. (f) Gorin, D. J.; Sherry, B. D.; Toste, F. D. *Chem. Rev.* **2008**, *108*, 3351−3378. (g) Jiménez-Núñez, E.; Echavarren, A. M. *Chem. Rev.* **2008**, *108*, 3326−3350. (h) Fürstner, A. *Chem. Soc. Rev.* **2009**, *38*, 3208−3221. (i) Krause, N.; Winter, C. *Chem. Rev.* **2011**, *111*, 1994−2009. (j) Corma, A.; Leyva-Peréz, A.; Sabater, M. J. *Chem. Rev.* **2011**, *111*, 1657−1712. (k) Raubenheimer, H. G.; Schmidbaur, H. *S. Afr. J. Sci.* **2011**, *107*, 31−43. (l) Gaillard, S.; Cazin, C. S. J.; Nolan, S. P. *Acc. Chem. Res.* **2012**, *45*, 778−787. (m) Hashmi, A. S. K. *Acc. Chem. Res.* **2014**, *47*, 864−876.

(2) Blanco Jaimes, M. C.; Hashmi, A. S. K. Gold-Catalyzed Oxygen-Atom Transfer to Alkynes. In *Modern Gold Catalyzed Synthesis*; Hashmi, A. S. K., Toste, F. D., Eds.; Wiley-VCH: Weinheim, Germany, 2012; pp 273−296.

(3) For recent reviews focused on the generation and synthetic utilization of gold(I) α-oxo carbenes, see: (a) Xiao, J.; Li, X. *Angew. Chem., Int. Ed.* **2011**, *50*, 7226−7236. (b) Zhang, L. *Acc. Chem. Res.* **2014**, *47*, 877−888. (c) Yeom, H.-S.; Shin, S. *Acc. Chem. Res.* **2014**, *47*, 966−977.

(4) For selected examples of oxidation reaction involving intramolecular trapping of gold(I) α-oxo carbenes, see: (a) Lu, Y.; Cui, L.; Zhang, G.; Zhang, L. *J. Am. Chem. Soc.* **2010**, *132*, 3258−3259. (b) Ye, L.; He, W.; Zhang, L. *J. Am. Chem. Soc.* **2010**, *132*, 8550−8551. (c) Ye, L.; He, W.; Zhang, L. *Angew. Chem., Int. Ed.* **2011**, *50*, 3236−3239. (d) Vasu, D.; Hung, H.-H.; Bhunia, S.; Gawade, S. A.; Das, A.; Liu, R.-S. *Angew. Chem., Int. Ed.* **2011**, *50*, 6911−6914. (e) Bhunia, S.; Ghorpade, S.; Huple, D. B.; Liu, R.-S. *Angew. Chem., Int. Ed.* **2012**, *51*, 2939−2942. (f) Wang, Y.; Ji, K.; Lan, S.; Zhang, L. *Angew. Chem., Int. Ed.* **2012**, *51*, 1915−1918. (g) Ghorpade, S.; Su, M.-D.; Liu, R.-S. *Angew. Chem., Int. Ed.* **2013**, *52*, 4229−4234. (h) Shi, S.; Wang, T.; Yang, W.; Rudolph, M.; Hashmi, A. S. K. *Chem.—Eur. J.* **2013**, *19*, 6576−6580. (i) Fu, J.; Shang, H.; Wang, Z.; Chang, L.; Shao, W.; Yang, Z.; Tang, Y. *Angew. Chem., Int. Ed.* **2013**, *52*, 4198−4202.

(5) For examples of an efficient intermolecular trapping of gold(I) α-oxo carbenes, see: (a) He, W.; Li, C.; Zhang, L. *J. Am. Chem. Soc.* **2011**, *133*, 8482−8485. (b) Davies, P. W.; Cremonesi, A.; Dumitrescu, L. *Angew. Chem., Int. Ed.* **2011**, *50*, 8931−8935. (c) Xiao, Y.; Zhang, L. *Org. Lett.* **2012**, *14*, 4662−4665. (d) Luo, Y.; Ji, K.; Li, Y.; Zhang, L. *J. Am. Chem. Soc.* **2012**, *134*, 17412−17415. (e) He, W.; Xie, L.; Xu, Y.; Xiang,

J.; Zhang, L. *Org. Biomol. Chem.* **2012**, *10*, 3168−3171. (f) Ji, K.; Zhao, Y.; Zhang, L. *Angew. Chem., Int. Ed.* **2013**, *52*, 6508−6512. (g) Wang, L.; Xie, X.; Liu, Y. *Angew. Chem., Int. Ed.* **2013**, *52*, 13302−13306. (h) Wu, C.; Liang, Z.; Yan, D.; He, W.; Xiang, J. *Synthesis* **2013**, *45*, 2605−2611. (i) Xie, L.; Liang, Z.; Yan, D.; He, W.; Xiang, J. *Synlett* **2013**, *24*, 1809−1812. (j) Li, J.; Ji, K.; Zheng, R.; Nelson, J.; Zhang, L. *Chem. Commun.* **2014**, *50*, 4130−4133. (k) Santos, M. D.; Davies, P. W. *Chem. Commun.* **2014**, *50*, 6001−6004.

(6) (a) Lu, B.; Li, C.; Zhang, L. *J. Am. Chem. Soc.* **2010**, *132*, 14070−14072. (b) Davies, P. W.; Cremonesi, A.; Martin, N. *Chem. Commun.* **2011**, *47*, 379−381.

(7) (a) Noey, E. L.; Luo, Y.; Zhang, L.; Houk, K. N. *J. Am. Chem. Soc.* **2012**, *134*, 1078−1084. (b) Lu, B.; Li, Y.; Wang, Y.; Aue, D. H.; Luo, Y.; Zhang, L. *J. Am. Chem. Soc.* **2013**, *135*, 8512−8524. (c) Henrion, G.; Chavas, T. E. J.; Le Goff, X.; Gagosz, F. *Angew. Chem., Int. Ed.* **2013**, *52*, 6277−6282.

(8) (a) Chen, P. *Angew. Chem., Int. Ed.* **2003**, *42*, 2832−2847. (b) Schröder, D. *Acc. Chem. Res.* **2012**, *45*, 1521−1532. (c) Zhu, W.; Yuan, Y.; Zhou, P.; Zeng, L.; Wang, H.; Tang, L.; Guo, B.; Chen, B. *Molecules* **2012**, *17*, 11507−11537.

(9) (a) Eyler, J. R. *Mass Spectrom. Rev.* **2009**, *28*, 448−467. (b) Polfer, N. C. *Chem. Soc. Rev.* **2011**, *40*, 2211−2221. (c) Roithová, J. *Chem. Soc. Rev.* **2012**, *41*, 547−559.

(10) For selected recent work, see: (a) Bythell, B. J.; Maître, P.; Paizs, B. *J. Am. Chem. Soc.* **2010**, *132*, 14766−14779. (b) Salpin, J.-Y.; Guillaumont, S.; Ortiz, D.; Tortajada, J.; Maître, P. *Inorg. Chem.* **2011**, *50*, 7769−7778. (c) Ortiz, D.; Blug, M.; Le Goff, X.-F.; Le Floch, P.; Mézailles, N.; Maître, P. *Organometallics* **2012**, *31*, 5975−5978. (d) Garand, E.; Fournier, J. A.; Kamrath, M. Z.; Schley, N. D.; Crabtree, R. H.; Johnson, M. A. *Phys. Chem. Chem. Phys.* **2012**, *14*, 10109−10113. (e) Dunbar, R. C.; Steill, J. D.; Polfer, N. C.; Oomens, J. *J. Phys. Chem. A* **2013**, *117*, 1094−1101. (f) De Petris, A.; Ciavardini, A.; Coletti, C.; Re, N.; Chiavarino, B.; Crestoni, M. E.; Fornarini, S. *J. Phys. Chem. Lett.* **2013**, *4*, 3631−3635.

(11) Kumar, P.; Roithová, J. *Eur. J. Mass Spectrom.* **2012**, *18*, 457−463.

(12) Zins, E. L.; Pepe, C.; Schröder, D. *J. Mass. Spectrom.* **2010**, *45*, 1253−1260.

(13) For selected papers utilizing this approach, see: (a) Remeš, M.; Roithová, J.; Schröder, D.; Cope, E. D.; Perera, C.; Senadheera, S. N.; Stensrud, K.; Ma, C.-C.; Givens, R. S. *J. Org. Chem.* **2011**, *76*, 2180−2186. (b) Shaffer, C. J.; Schröder, D.; Gütz, C.; Lützen, A. *Angew. Chem., Int. Ed.* **2012**, *51*, 8097−8100. (c) Tsybizova, A.; Rulíšek, L.; Schröder, D.; Rokob, T. A. *J. Phys. Chem. A* **2013**, *117*, 1171−1180. (d) Hývl, J.; Roithová, J. *Org. Lett.* **2014**, *16*, 200−203.

(14) Ortega, J. M.; Glotin, F.; Prazers, R. *Infrared Phys. Technol.* **2006**, *49*, 133−138.

(15) Mac Aleese, L.; Maître, P. *Mass Spectrom. Rev.* **2007**, *26*, 583−605.

(16) (a) Perdew, J. P.; Chevary, J. A.; Vosko, S. H.; Jackson, K. A.; Pederson, M. R.; Singh, D. J.; Fiolhais, C. *Phys. Rev. B: Condens. Matter Mater. Phys.* **1992**, *46*, 6671−6687. (b) Perdew, J. P.; Chevary, J. A.; Vosko, S. H.; Jackson, K. A.; Pederson, M. R.; Singh, D. J.; Fiolhais, C. *Phys. Rev. B: Condens. Matter Mater. Phys.* **1993**, *48*, 4978. (c) Perdew, J. P.; Burke, K.; Wang, Y. *Phys. Rev. B: Condens. Matter Mater. Phys.* **1996**, *54*, 16533−16539. (d) Adamo, C.; Barone, V. *J. Chem. Phys.* **1998**, *108*, 664−675.

(17) Frisch, M. J.; et al. *Gaussian 09*, Revision A.02; Gaussian, Inc.: Wallingford, CT, 2009.

(18) Scott, A. P.; Radom, L. *J. Phys. Chem.* **1996**, *100*, 16502−16513.

(19) Škríba, A.; Jašíková, L.; Roithová, J. *Int. J. Mass Spectrom.* **2012**, *330*, 226−232.

(20) Such a type of gold(I) benzylidene complexes has been reported previously: (a) Fedorov, A.; Batiste, L.; Bach, A.; Birney, D. M.; Chen, P. *J. Am. Chem. Soc.* **2011**, *133*, 12162−12171. (b) Batiste, L.; Fedorov, A.; Chen, P. *Chem. Comun.* **2010**, *46*, 3899−3901.

(21) Kirmse, W. *Eur. J. Org. Chem.* **2002**, 2193−2256.

(22) See: Kumar, P.; Troast, D. M.; Cella, R.; Louie, J. *J. Am. Chem. Soc.* **2011**, *133*, 7719−7721 and references cited therein.

(23) Bouma, W. J.; Nobes, R. H.; Radom, L.; Woodward, C. E. *J. Org. Chem.* **1982**, *47*, 1869−1875.

(24) For recent examples, see: (a) Chiavarino, B.; Crestoni, M. E.; Fornarini, S.; Lanucara, F.; Lemaire, J.; Maître, P.; Scuderi, D. *Chem.—Eur. J.* **2009**, *15*, 8185−8195. (b) Salpin, J.-Y.; Guillaumont, S.; Ortiz, D.; Tortajada, J.; Maître, P. *Inorg. Chem.* **2011**, *50*, 7769−7778. (c) Garand, E.; Fournier, J. A.; Kamrath, M. Z.; Schley, N. D.; Crabtree, R. H.; Johnson, M. A. *Phys. Chem. Chem. Phys.* **2012**, *14*, 10109−10113. (d) Dunbar, R. C.; Steill, J. D.; Polfer, N. C.; Oomens, J. *J. Phys. Chem. A* **2013**, *117*, 1094−1101. (e) De Petris, A.; Ciavardini, A.; Coletti, C.; Re, N.; Chiavarino, B.; Crestoni, M. E.; Fornarini, S. *J. Phys. Chem. Lett.* **2013**, *4*, 3631−3635.

(25) Oomens, J.; Sartakov, B. G.; Meijer, G.; von Helden, G. *Int. J. Mass Spectrom.* **2006**, *254*, 1−19.

(26) Beller, M.; Seayad, J.; Tillack, A.; Jiao, H. *Angew. Chem., Int. Ed.* **2004**, *43*, 3368−3398.

(27) Geoffery, G. L.; Bassner, S. L. *Adv. Organomet. Chem.* **1988**, *28*, 1−83.

(28) (a) Grotjahn, D. B.; Bikzhanova, G. A.; Collins, L. S. B.; Concolino, T.; Lam, K.-C.; Rheingold, A. L. *J. Am. Chem. Soc.* **2000**, *122*, 5222−5223. (b) Grotjahn, D. B.; Collins, L. S. B.; Wolpert, M.; Bikzhanova, G. A.; Lo, H. C.; Combs, D.; Hubbard, J. L. *J. Am. Chem. Soc.* **2001**, *123*, 8260−8270. (c) Hofmann, P.; Perez-Moya, L. A.; Steigelmann, O.; Riede, J. *Organometallics* **1992**, *11*, 1167−1176.

(29) Similarly to the earlier report on interaction of gold(I) cation $[(Me_3P)Au]^+$ with unsaturated hydrocarbons our attempts to locate potential energy minimum for h^6 arene-coordinated structure failed. See: Jašíková, L.; Roithová, J. *Organometallics* **2012**, *31*, 1935−1942.

(30) Tsierkezos, N. G.; Roithová, J.; Schröder, D.; Ončák, M.; Slavíček, P. *Inorg. Chem.* **2009**, *48*, 6287−6296.